Supplementary Information

Evaluation of Fuel Properties of Hydrothermal Carbonization-derived Shrimp Shell Hydrochar

Swarna Saha, Md Tahmid Islam, Joshua Calhoun, and M. Toufiq Reza*

Department of Biomedical and Chemical Engineering and Sciences, Florida Institute of Technology, Melbourne, FL 32901, USA

* Corresponding Author: email: treza@fit.edu, phone: +1-321-674-8578

Table Caption

TableS 1 Slagging, fouling, sagging viscosity and alkali indices, Cl content equation and limit for detection.

Figure captions

FigureS1 FTIR spectra for raw SS and hydrochar at different temperature.

FigureS2 TG thermogram results for raw SS and hydrochars at different temperatures.

TableS 1 Slagging, fouling, sagging viscosity and alkali indices, Cl content equation and limit for detection [1].

Slagging /fouling index	Equation	Limit
Slagging Index	SI =(B/A) ×wt.% S in dry fuel	SI < 0.6 low slagging inclination SI =0.6 to 2.0 medium SI = 2.0 to 2.6 high SI > 2.6 extremely high
Fouling Index	FI= (B/A) × (Na_2O + K_2O)	FI ≤0.6 lower fouling inclination 0.6 < FI < 40 medium FI ≥ 40 high
Slagging Viscosity Index	SV= (SiO_2×100)/ (SiO_2 + MgO + CaO+ Fe_2O_3)	SV > 72 low slagging inclination 65 ≤ SV ≤ 72 moderate SV < 65 high
Alkali Index	AI= (Na_2O + K_2O) in kg/GJ	0.17 < A I< 0.34 slagging/fouling probable AI ≥ 0.34 slagging/fouling is certain
Chlorine Content	Cl as received (%)	Cl < 0.2-0.3 low slagging inclination 0.2 < Cl < 0.3 medium 0.3 < Cl < 0.5 high Cl > 0.5 extremely high

FTIR Result Analysis

The FTIR spectra of raw shrimp shell (SS) to hydrochars at various temperatures are displayed in **Figure S1**, which gives a qualitative overview of the surface functionalities present in the samples. All of the samples displayed two adsorption peaks at 2923 cm^{-1} and 2855 cm^{-1}, ascribed from C-H asymmetric and symmetric axial deformation in CH_2 due to the existence of aliphatic structures derived from lipids in SS, respectively [2-4]. However, a peak at around 1650 cm^{-1} was seen only for SS-110 which is attributed from amide I (C═O) and N-H angular deformation in primary amine and showed non-existent immergence for other hydrochar samples[2, 5]. Except for the raw SS, another persistent peak at 1620 cm^{-1} corresponds to N-H angular deformation in NH_2-R for all hydrochars at different temperatures [6]. A prominent peak at 1500 cm^{-1} and 1455 cm^{-1} could be ascribed for N-H angular deformation on secondary amine [2, 7] and C=C-C axial deformation in aromatic C_6H_5- R [2], respectively. The intensity of the peak at 1010 cm^{-1} due to C-H in-plane angular deformation in aromatic C_6H_5- R increased as it changed from raw SS to hydrochar [8]. A negligible peak at 890 cm^{-1} corresponding to $\beta - 1, 4$ glycosidic bonds for raw SS showed increasing intensity with higher HTC temperature which indicates the long aliphatic bond in raw SS breaks further with increasing HTC temperature [5, 9]. A similar trend was followed by the peak found for 700 cm^{-1} owing to O-H angular deformation in alcohol [10, 11]. Finally, two peaks displayed at 600 cm^{-1} and 550 cm^{-1} for all the hydrochars are attributed from S-S and C-S axial deformation in disulfides, respectively [2, 4]. These above-mentioned peaks are all comparable to prior experimental findings conducted on raw SS and hydrochars [4, 5, 12].

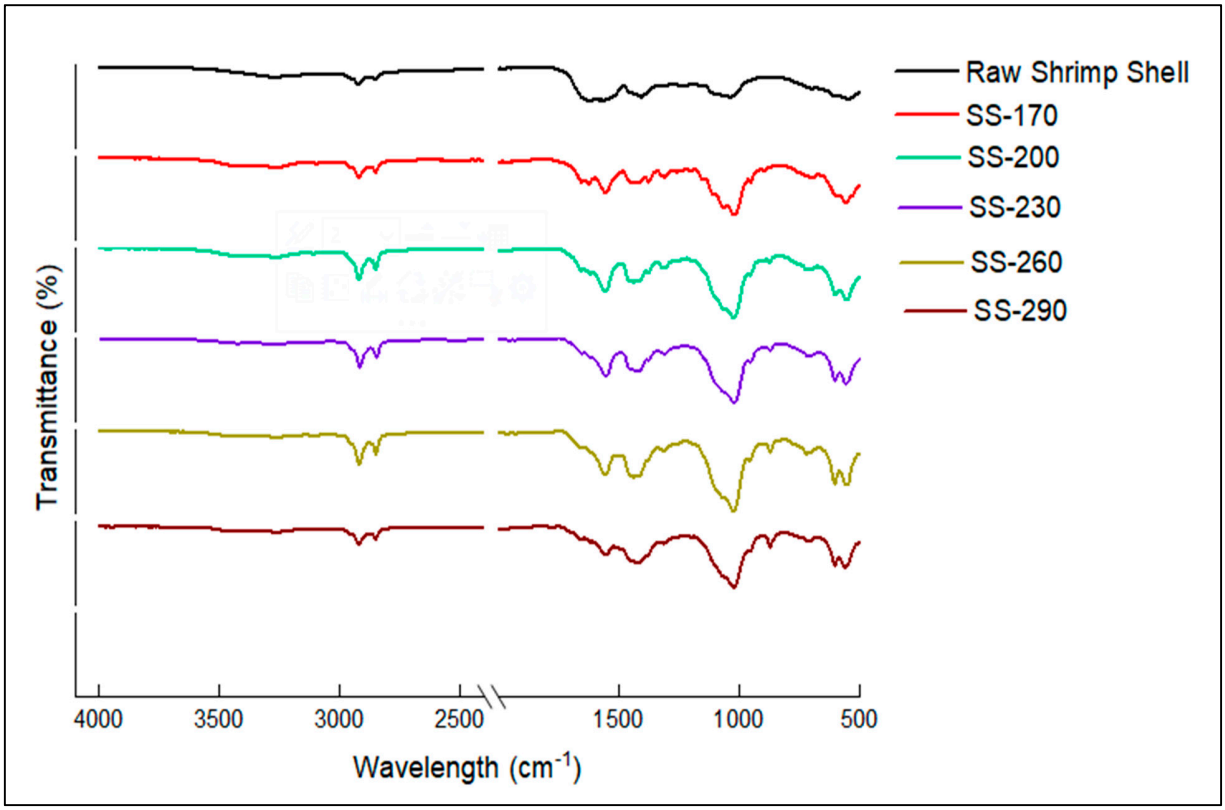

FigureS3 *FTIR spectra for raw SS and hydrochar at different temperature.*

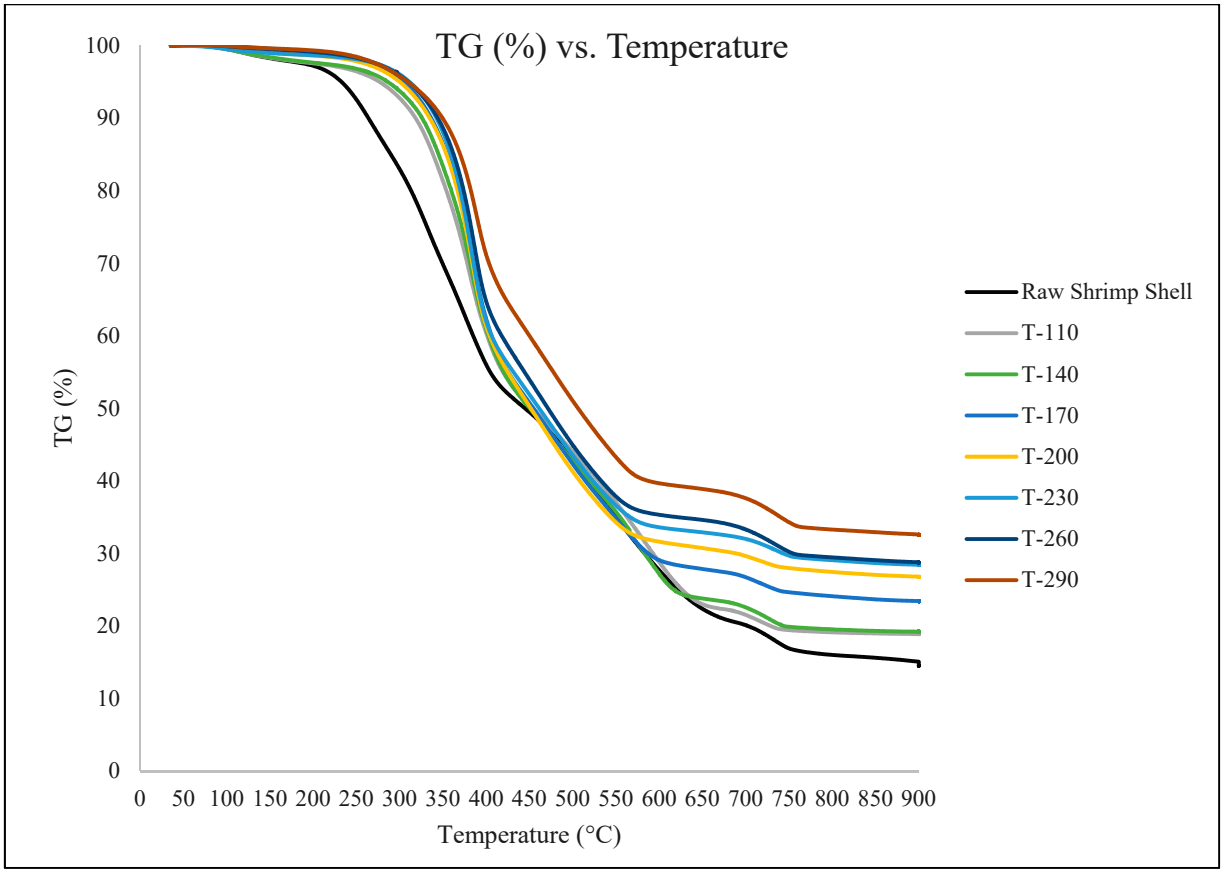

FigureS4 TG thermogram results for raw SS and hydrochars at different temperatures.

References

1. Tortosa Masiá, A.A., et al., *Characterising ash of biomass and waste.* Fuel Processing Technology, 2007. **88**(11-12): p. 1071-1081.
2. Coates, J., *Interpretation of Infrared Spectra, A Practical Approach*, in *Encyclopedia of Analytical Chemistry*. 2006.
3. Zhang, Y., et al., *Controlled assembly of Fe3O4 magnetic nanoparticles on graphene oxide.* Nanoscale, 2011. **3**(4): p. 1446-1450.
4. Kannan, S., Y. Gariepy, and G.S.V. Raghavan, *Optimization and Characterization of Hydrochar Derived from Shrimp Waste.* Energy & Fuels, 2017. **31**(4): p. 4068-4077.
5. He, C., et al., *Waste shrimp shell-derived hydrochar as an emergent material for methyl orange removal in aqueous solutions.* Environ Int, 2020. **134**: p. 105340.
6. Allison, G.G., et al., *Measurement of key compositional parameters in two species of energy grass by Fourier transform infrared spectroscopy.* (1873-2976 (Electronic)).
7. Donald L. Pavia, G.M.L., George S. Kriz, James A. Vyvyan, *Introduction to Spectroscopy*.
8. El Ichi, S., et al., *Chitosan improves stability of carbon nanotube biocathodes for glucose biofuel cells.* Chemical Communications, 2014. **50**(93): p. 14535-14538.
9. Wysokowski, M., et al., *Modification of chitin with kraft lignin and development of new biosorbents for removal of cadmium(II) and nickel(II) ions.* (1660-3397 (Electronic)).
10. Chen, B., D. Zhou, and L. Zhu, *Transitional Adsorption and Partition of Nonpolar and Polar Aromatic Contaminants by Biochars of Pine Needles with Different Pyrolytic Temperatures.* Environmental Science & Technology, 2008. **42**(14): p. 5137-5143.
11. Hong, P.-Z., et al., *Thermogravimetric analysis of chitosan.* Journal of Applied Polymer Science, 2007. **105**(2): p. 547-551.
12. Kannan, S., Y. Gariepy, and G.S.V. Raghavan, *Conventional Hydrothermal Carbonization of Shrimp Waste.* Energy & Fuels, 2018. **32**(3): p. 3532-3542.